# Urea-Functionalized Silver Catalyst toward Efficient and Robust $CO_2$ Electrolysis with Relieved Reliance on Alkali Cations

Garg, Sahil; Li, Mengran; Hussain, Tanveer; Idros, Mohamed Nazmi; Wu, Yuming; Zhao, Xiu Song; Wang, Geoff G.X.; Rufford, Thomas E.

**DOI**
10.1021/acsami.2c05918

**Publication date**
2022

**Document Version**
Final published version

**Published in**
ACS applied materials & interfaces

ACS APPLIED MATERIALS & INTERFACES

www.acsami.org

Research Article

# Urea-Functionalized Silver Catalyst toward Efficient and Robust $CO_2$ Electrolysis with Relieved Reliance on Alkali Cations

Sahil Garg, Mengran Li,* Tanveer Hussain, Mohamed Nazmi Idros, Yuming Wu, Xiu Song Zhao, Geoff G. X. Wang, and Thomas E. Rufford*

Cite This: *ACS Appl. Mater. Interfaces* 2022, 14, 35504–35512

Read Online

ACCESS | Metrics & More | Article Recommendations | Supporting Information

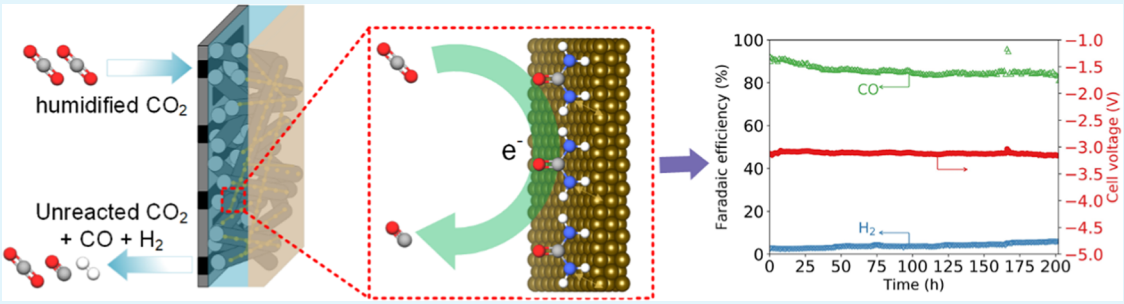


**ABSTRACT:** We report a new strategy to improve the reactivity and durability of a membrane electrode assembly (MEA)-type electrolyzer for $CO_2$ electrolysis to CO by modifying the silver catalyst layer with urea. Our experimental and theoretical results show that mixing urea with the silver catalyst can promote electrochemical $CO_2$ reduction ($CO_2R$), relieve limitations of alkali cation transport from the anolyte, and mitigate salt precipitation in the gas diffusion electrode in long-term stability tests. In a 10 mM $KHCO_3$ anolyte, the urea-modified Ag catalyst achieved CO selectivity 1.3 times better with energy efficiency 2.8-fold better than an untreated Ag catalyst, and operated stably at 100 mA $cm^{-2}$ with a faradaic efficiency for CO above 85% for 200 h. Our work provides an alternative approach to fabricating catalyst interfaces in MEAs by modifying the catalyst structure and the local reaction environment for critical electrochemical applications such as $CO_2$ electrolysis and fuel cells.

**KEYWORDS:** *$CO_2$ utilization, urea, electrocatalyst, silver nanoparticles, vapor-fed electrolyzer, membrane electrode assembly*



## 1. INTRODUCTION

Electrochemical $CO_2$ reduction ($CO_2R$) technologies show promise to convert $CO_2$ to chemical feedstocks and fuels using renewable electricity.[1,2] Of the various designs for $CO_2$ electrolyzers, membrane electrode assembly (MEA) designs, or zero-gap electrolyzers, are emerging as one of the $CO_2R$ technologies that can achieve high product selectivity at high current densities.[3−9] A core advantage of MEA electrolyzers is that these designs do not have a bulk, flowing catholyte between the cathode and the ion exchange membrane, which significantly reduces ohmic losses in the electrolyzer and thus enhances the overall energy efficiency of $CO_2R$.[9] However, the absence of the catholyte can also lead to poor stability due to salt precipitation in the cathode gas diffusion electrode (GDE), and if there are insufficient alkali cations available at the cathode, $CO_2R$ selection may be reduced.[6,10,11] Both these issues originate from the strong reliance of MEA electrolyzers on alkali cations (e.g., $K^+$) for active $CO_2R$.[10]

Only a few engineering solutions have been reported to resolve these critical issues, including (i) using pure water as the anolyte with the periodic injection of salt solutions to the cathode,[5] (ii) periodic flushing of the GDE with pure water to wash away the salts,[6] or (iii) alternating cell voltages to minimize $OH^-$ concentration at the interface.[12] However, these approaches all involve unsteady-state and periodic interventions that disrupt electrolyzer operations, which lead to poor overall process efficiency, increased complexity of process control infrastructure, and increased costs.

An alternative approach that is yet to be fully explored is to promote $CO_2R$ catalysts with molecular modifiers such as urea or ionic liquids.[13−18] There is evidence that urea or ionic liquids can influence catalyst activity and selectivity through optimizing catalyst structures and local reaction environments. These modifier molecules can have effects such as (i) stabilizing $CO_2R$ reaction intermediate species such as *COOH,[19,20] (ii) altering catalyst local proton availability by increasing hydrophobicity or decreasing the dielectric constant

Received: April 4, 2022
Accepted: July 24, 2022
Published: August 1, 2022

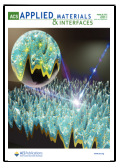




https://doi.org/10.1021/acsami.2c05918
*ACS Appl. Mater. Interfaces* 2022, 14, 35504−35512

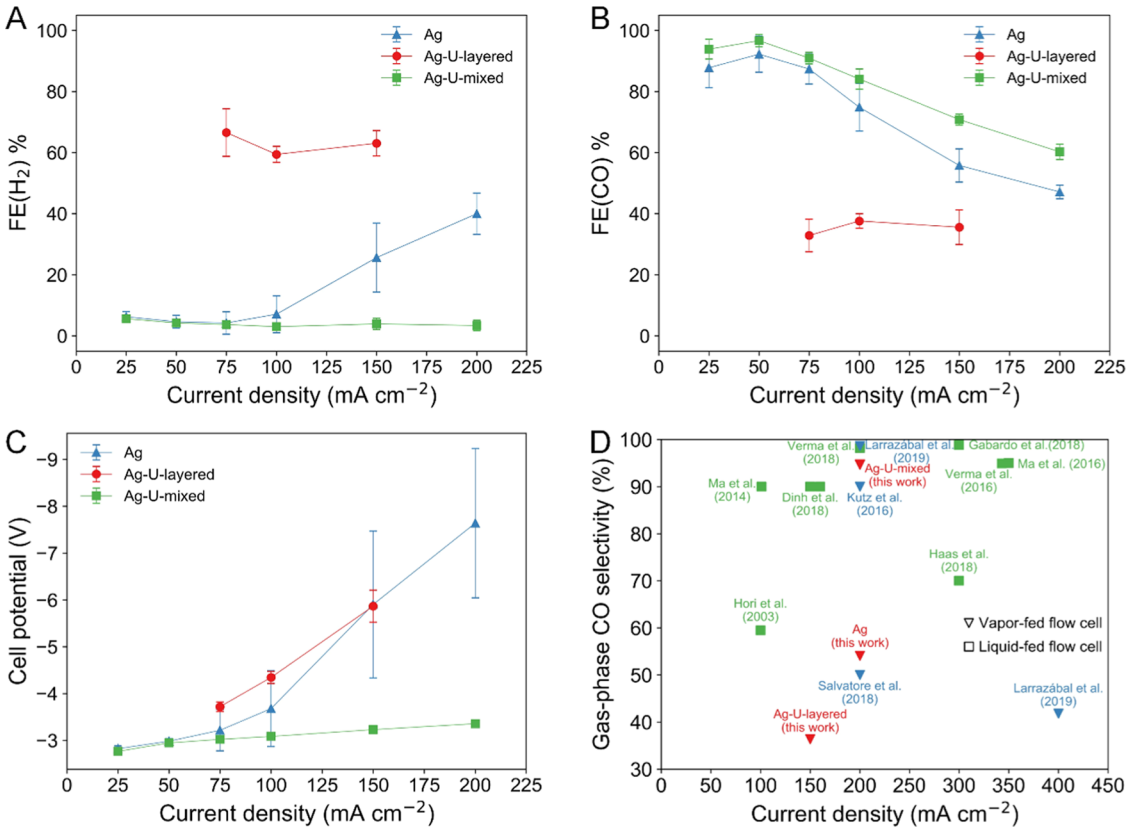


**Figure 1.** Comparison of the faradaic efficiencies of (A) $H_2$, (B) CO, and (C) cell potentials for $CO_2$ electrolysis in the MEA electrolyzer using Ag GDE, Ag-U-layered GDE, and A-U-mixed GDE with equivalent of 1 ± 0.05 mg $cm^{-2}$ Ag loadings. Error bars show the standard deviation of three separate experiments. (D) The landscape of current density versus CO selectivity in gaseous products for liquid-fed flow electrolyzers and vapor-fed electrolyzers (MEA electrolyzers) with Ag-based cathodes. We only include here results reported at a total current density higher than 100 mA·$cm^{-2}$. The details of the literature presented in (D) are provided in Table S1 in the Supporting Information.

in the electric double layer,[21−24] (iii) optimizing the catalyst electronic structure for $CO_2R$,[20,25] and (iv) restructuring the catalyst surface to allow exposure of more active sites for $CO_2R$ and increase of local pH to suppress HER.[26] We expect these molecules to promote the catalytic activity in the MEA cells while reducing their dependency on alkali cations.

In this study, urea is immobilized in the silver catalyst layer of the cathode GDE in the MEA electrolyzer by mixing urea with silver nanoparticles before catalyst deposition (Figure S1). We chose urea in this work because in our earlier work with catholyte-fed electrolyzers,[18] urea proved effective in modifying the Ag surface and promoting $CO_2R$ to CO. In this paper, we report that the inclusion of urea in the catalyst layer enabled the MEA to operate efficiently with a dilute 10 mM $KHCO_3$ anolyte. Our experimental and theoretical results unveil that the amino group ($-NH_2$) of urea can bind strongly with the silver surface, which could promote $CO_2R$ performance by stabilizing the *COOH intermediate and suppressing the hydrogen evolution reaction (HER). Consequently, the urea-modified cathode achieved a stable $FE_{CO}$ above 85% at 100 mA·$cm^{-2}$ for 200 h in an MEA configuration with 10 mM $KHCO_3$ as the anolyte. Our work demonstrates an alternative approach to circumvent the long-lasting issues of MEA-based electrochemical processes by modifying the catalyst structure and the local reaction environment with molecular modifiers.

## 2. METHODS

**2.1. Preparation of the Catalyst Ink and Gas Diffusion Electrodes.** We prepared several Ag-based gas diffusion electrodes (GDEs) with different catalyst inks. The benchmark catalyst ink had 100 mg of Ag nanoparticles (NPs, 20−40 nm) from Alfa Aesar mixed with 100 μL of polytetrafluoroethylene (PTFE, 60 wt % dispersion in water diluted to 6 wt %) and 8 mL of isopropyl alcohol (IPA, ≥99.7%, Sigma-Aldrich). The catalyst ink was sonicated for 30 min and then deposited onto a commercial gas diffusion layer (GDL 240, Fuel Cell Store) by spray-coating (RS pro airbrush kit, RS components) until an Ag catalyst loading of 1 ± 0.05 mg·$cm^{-2}$ was achieved. We refer to this benchmark, untreated Ag-based cathode as Ag GDE (Figure S1).

We prepared urea-modified Ag GDEs using urea (≥99.5%, Sigma-Aldrich) by two different methods. In method 1, the Ag-U-layered GDE (Figure S1) was prepared by spray-coating a solution of 1 g of urea in 4 mL of water and 4 mL of IPA onto the already prepared Ag GDE to achieve a 0.5 ± 0.05 mg·$cm^{-2}$ loading of urea. In method 2, the Ag-U-mixed GDE was prepared by mixing 100 mg of Ag NPs, 50 mg of urea pellets, and 100 μL of PTFE (6 wt % in water) in 4 mL of water and 4 mL of IPA. This mixture was sonicated for 30 min and then spray-coated directly on GDL 240. The total loading of ink on the Ag-U-mixed GDE was 1.5 ± 0.05 mg·$cm^{-2}$ to achieve a silver loading of 1 mg·$cm^{-2}$ and a urea loading of 0.5 mg·$cm^{-2}$. Prior work by others[27] used similar "layered" and "mixed" methods with multiwalled carbon nanotubes and the Ag catalyst for $CO_2R$. Although the spray-coating method in our study is similar to that in prior work, the role of urea is not the same as that of carbon nanotubes because (1) urea serves as a molecular modifier to limit proton availability and strengthen binding with $CO_2R$ intermediates and (2) water is limited at the catalyst-membrane interface so that a high concentration of urea can be maintained close to the catalyst surface.

**2.2. $CO_2$ Electrolyzer Assembly and Operation.** We purchased a 5 $cm^2$ $CO_2$ electrolyzer from Dioxide Materials (Figure S2) with a humified $CO_2$ gas chamber and an anolyte chamber with an $IrO_2$-


https://doi.org/10.1021/acsami.2c05918
ACS Appl. Mater. Interfaces 2022, 14, 35504−35512

based GDE (Dioxide Materials). We pumped 10 mM $KHCO_3$ (≥99.5%, Sigma-Aldrich) at a rate of 1 ml·min$^{-1}$ through the serpentine flow field of the anode-side endplate. The anode and the cathode were separated by an anion exchange membrane (AEM Sustainion, X37-50 grade, Dioxide Materials). Humidified $CO_2$ at temperature = 20 ± 3 °C was supplied to the cathode GDE at a flow rate of 60 sccm (unless stated otherwise) using a mass flow controller (pMFC, MKS instruments, ±1% precision). The catalyst layers on the anode and the cathode each faced the AEM.

Electrochemical measurements were conducted at ambient temperature and pressure using an Autolab PGSTAT302N potentiostat in a two-electrode configuration. The $CO_2$ electrolyzer was tested using a galvanostatic mode at current densities (CD) from 25 to 200 mA·cm$^{-2}$. The flow rate of the effluent gas (unreacted $CO_2$ + gas products) from the cathode cell was measured with a digital flowmeter (Optiflow 520, Sigma-Aldrich, ±3% resolution). At each CD, the gas products were analyzed using a gas chromatograph (GC 2030, Shimadzu) equipped with a thermal conductivity detector (TCD), a flame ionization detector (FID), and a packed column (Shincarbon). The first gas sample was analyzed after 500 s or when the cell voltage became stable (whichever was later). At least three different gas injections were analyzed at regular intervals, and an average value was reported. We report all cell voltages here as the average cell potential recorded over time intervals of at least 100 s at each CD. No *i*R-correction was applied to the reported voltage values. Ohmic and charge transfer resistance was determined by galvanostatic electrochemical impedance spectroscopy (EIS) at frequencies ranging from 100 kHz to 1 Hz, recording twice per decade.

The faradaic efficiency (FE) of the gaseous products (P) was determined using the following equation

$$\mathrm{FE_P} = \frac{z_\mathrm{P}\cdot F\cdot N_\mathrm{P}}{I} \times 100 \quad (1)$$

where $z_\mathrm{P}$ is the number of electrons required for a given product (P), $F$ is Faraday's constant, $N_\mathrm{P}$ is the molar flow rate of the gas product calculated from the GC and the effluent gas flow rate, and $I$ is the current applied.

The energy efficiency ($\mathrm{EE_{CO}}$) of $CO_2$R to CO was calculated using the following equation

$$\mathrm{EE_{CO}} = \frac{\mathrm{FE_{CO}}\cdot E_\mathrm{eq,cell}}{E_\mathrm{cell}} \quad (2)$$

where $E_\mathrm{eq,cell}$ is standard cell potential (−1.34 V) for $CO_2$R to CO coupled with the $O_2$ evolution reaction at the anode, and $E_\mathrm{cell}$ is the actual cell potential.

For the long-term electrode durability test, a constant current density of 100 mA·cm$^{-2}$ was applied across the electrolyzer. The cell potential was monitored and $\mathrm{FE_{CO}}$ was calculated every 1 h.

**2.3. Characterization.** Scanning electron microscopy (SEM) of GDEs before and after $CO_2$R experiments was performed on a JOEL JSM-7100 or JSM-7001 field emission microscope. X-ray photoelectron spectroscopy (XPS) was obtained with a Kratos Axis Ultra XPS spectrometer using a monochromatic Al K$\alpha$ radiation (1486.6 eV) source for excitation. CASA software was used to process and calibrate all of the XPS spectra using the carbon (C) 1s peak at 284.6 eV. Raman data were collected using a Renshaw Raman microscope equipped with 514 and 785 nm lasers. Raman measurements were acquired using a 514 nm laser (unless stated otherwise) and the laser power was regulated between 10 to 100 mW to acquire sufficient signals for the spectra. We used Spectragryph software for analysis and baseline correction for all of the Raman Spectra.

## 3. RESULTS AND DISCUSSION

**3.1. Performance of MEA Cells with the Urea-Embedded Silver Catalyst.** Figure 1A,B shows the faradaic efficiencies of $H_2$ ($\mathrm{FE_{H2}}$) and CO ($\mathrm{FE_{CO}}$) of the MEA electrolyzers with the untreated Ag GDE, Ag-U-mixed GDE, and Ag-U-layered GDE. We repeated each test at least three times and reported the mean $\mathrm{FE_P}$ values with error bars showing the standard deviation. As shown in Figure 1A,B, the Ag-U-mixed cell shows a significant improvement in $\mathrm{FE_{CO}}$ and suppression of unwanted HER at higher current densities. For example, at a CD of 150 mA·cm$^{-2}$, the Ag-U-mixed GDE achieved a $\mathrm{FE_{CO}}$ of 71.86 ± 0.09%, which is far higher than those for the untreated Ag GDE ($\mathrm{FE_{CO}}$ = 50.81 ± 2.43%) and the Ag-U-layered GDE ($\mathrm{FE_{CO}}$ = 35.55 ± 4.90%). $\mathrm{FE_{H_2}}$ remained below 10% for the Ag-U-mixed GDE but was up to $\mathrm{FE_{H_2}}$ = 40% at 200 mA·cm$^{-2}$ for the untreated Ag GDE. The HER is the dominant reaction for the Ag-U-layered cells, where $\mathrm{FE_{CO}}$ is the lowest among the cell tests. The large difference in $CO_2$R selectivity to CO between Ag-U-mixed and Ag-U-layered cells indicates that urea may have a critical effect on the local reaction environment and or state of the Ag catalyst at active sites.

Additionally, the total faradaic efficiency (CO + $H_2$) decreases with the current density in Ag-U-mixed cells (Figure S3). We anticipate that the loss of faradaic efficiencies in both Ag-U-mixed and Ag cells at high rates may relate to the crossover of formate ions through the AEM and subsequent oxidation of the formate ions at the anode.[28,29] We confirmed trace concentrations of formate ions in the anolyte by NMR after the $CO_2$R test (Figure S4). We also ruled out the decomposition of urea to CO, or $CO_2$, as a contributor to the $\mathrm{FE_{CO}}$ results by performing electrolysis with a Ag-U-mixed GDE fed with argon gas. Figure S5 shows that in the absence of a $CO_2$ gas feed, we observed 100% $\mathrm{FE_{H2}}$, and from this, we infer that urea did not decompose to CO at the conditions used for $CO_2$R. This control experiment also confirms that the increase in $\mathrm{FE_{CO}}$ over Ag-U-mixed cells during $CO_2$R only originates from the reduction of $CO_2$.

Figure 1C shows clearly that urea in the GDE catalyst layer has a profound impact on the overall cell potentials. The cell potentials of the Ag-U-mixed GDE electrolyzer increase from 2.789 ± 0.055 V at 25 mA·cm$^{-2}$ to 3.359 ± 0.048 V at 200 mA·cm$^{-2}$, and these cell potentials are much lower than that for the untreated Ag GDE (7.640 ± 1.594 V at 200 mA·cm$^{-2}$). We note that 7.640 V is a relatively large cell potential here, and this result is partly because of the low concentration anolyte (0.1 mM) used in these experiments. This observation further highlights the significance of the cell potentials observed for the Ag-U-mixed GDE and suggests that in addition to the effects on $CO_2$R selectivity, urea also affects the required overpotentials at high current densities. The significance of this result is that the overall $CO_2$ conversion energy efficiency of the electrolyzer improved from 8.60 ± 1.88% in untreated Ag cells to 24.04 ± 1.11% in Ag-U-mixed cells at 200 mA·cm$^{-2}$ (Figure S6).

Figure 1D and Table S1 summarize a few recent reports of CO selectivity in the gaseous products (CO + $H_2$) in vapor-fed MEA electrolyzers and liquid-fed electrolyzers. Although the Ag-U-mixed cell performance is not at the top right corner of Figure 1D (i.e., high CO selectivity in gaseous products at high current densities), our result ranks among the highest reported CO selectivity in the gaseous products at high current densities reported in an MEA electrolyzer.

By varying catalyst loading from 0.75 to 1.5 mg·cm$^{-2}$ for the Ag-U-mixed cells, as shown in Figure S7, we observed no discernable changes in cell potentials and $\mathrm{FE_{H_2}}$ when changing catalyst loading. There is only a slightly lower $\mathrm{FE_{CO}}$ value for 0.75 mg·cm$^{-2}$ than that for 1.5 mg·cm$^{-2}$, which results from


https://doi.org/10.1021/acsami.2c05918
ACS Appl. Mater. Interfaces 2022, 14, 35504−35512

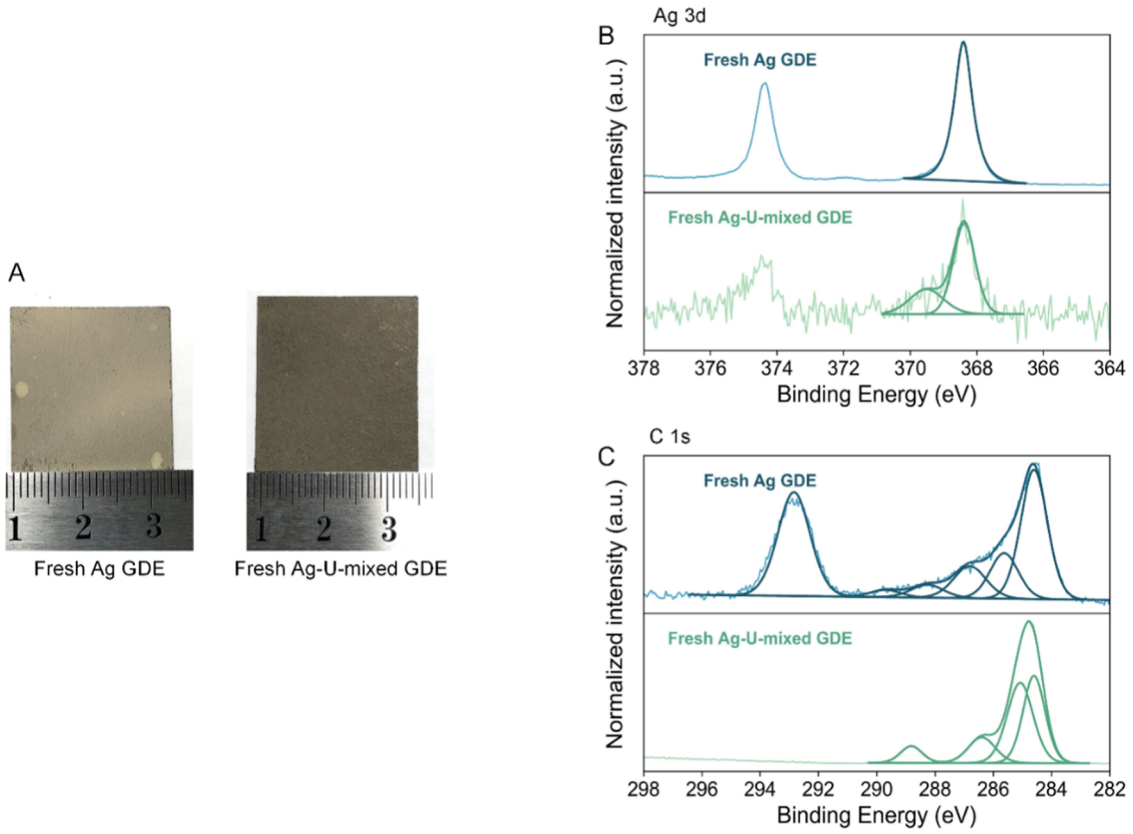


**Figure 2.** Images of freshly prepared (A) Ag electrode and Ag-U-mixed electrode; high-resolution XPS spectra of (B) Ag 3d and (C) C 1s on the fresh Ag and fresh Ag-U-mixed electrodes. The raw spectra are shown with light-colored lines, while the analogous fitted and deconvoluted peaks are shown with dark-colored lines.

the reduced number of active sites for $CO_2R$. The $FE_{H_2}$ values of all of the Ag-U-mixed cells with different catalyst loadings remain lower than those of the untreated Ag cells (see Figures S7 and 1A), further confirming the effective role of urea in suppressing HER in the MEA cells using 10 mM $KHCO_3$.

**3.2. Role of Urea in Catalyst Activation for $CO_2R$.** Our previous work reported that urea can be specifically adsorbed on the Ag surface and enhances CO production by stabilizing the $CO_2R$ intermediates.[18] Therefore, in the Ag-U-mixed GDE, we believe that urea may interact strongly with the Ag catalyst and promote efficient $CO_2$ reduction. We examined the surface of the catalyst layer of untreated Ag and Ag-U-mixed samples visually and with XPS. We observed that the Ag-U-mixed GDE is darker compared to the untreated Ag GDE, and the urea-modified catalyst layer had a greenish tinge (Figure 2A). The uniform distribution of Ag nanoparticles from SEM images (Figure S8) indicates that the color difference is not from differences in the morphology. Instead, the XPS data show that the color change is due to chemical interactions. The Ag 3d XPS spectra shown in Figure 2B for the Ag-U-mixed electrode exhibit two distinctive deconvoluted peaks at 368.4[30] and 369.5 eV,[31] which correspond to the features of Ag and Ag organic amine, respectively. In contrast, the Ag 3d spectra for the Ag electrode only show a single Ag metallic peak at 368.4 eV. The presence of an Ag organic amine peak suggests bonding between the Ag surface and the amino groups of urea.

The C 1s spectra of the Ag electrode have deconvoluted peaks for graphitic carbon at 284.6 eV;[32] carbon contamination at 285.6, 286.8, and 288.3 V;[32,33] and fluorinated carbons at 289.7 and 292.8 eV (due to PTFE in the catalyst layer).[34,35] However, the Ag-U-mixed GDE exhibits two additional peaks at 286.3 and 288.7 eV, corresponding to $C-NH_2$ and C═O, respectively.[36] The atomic percentages of $C-NH_2$ and C═O on the Ag-U-mixed surface are 13.57 and 7.14 (almost 2:1 ratio), which is in good agreement with the 2:1 ratio of $-NH_2$ and C═O groups in urea. The N 1s XPS peaks of the Ag-U-mixed GDE (shown in Figure S9) at 399.2 and 400.0 eV can be assigned to $C-NH_2$[36] and Ag organic amine,[37] respectively.

The C 1s and Ag 3d XPS data confirm the availability of urea on the Ag-U-mixed electrode surface and its chemical interactions with the Ag catalyst. The availability of urea in Ag-U-mixed GDE may enable stabilization of $CO_2$ electrolysis intermediate species and suppress HER (Figure 1A). Several groups such as Ahn et al.[38] and Cao et al.[39] reported that amino groups on the electrode surface facilitate the stabilization of $CO_2R$ intermediates (e.g., *COOH) through hydrogen bonding, thereby improving the $CO_2R$ performance. In addition, Kim et al.[19] proposed that the adsorbed amine molecules on Ag can destabilize the *H binding, which inhibits the HER.

The characterization of the catalyst layers by XPS after $CO_2R$ may provide further information about the interactions during $CO_2R$. Unfortunately, the XPS of the used catalyst from an MEA electrolyzer is unlikely to be useful in this case because the intimate contact of the catalyst layer and the membrane in the MEA leads to delamination of the Ag-U-mixed catalyst when the electrolyzer is dissembled (see Figure S10). Instead, we used Raman spectroscopy to compare the interactions between urea and Ag nanoparticles in the Ag-U-


https://doi.org/10.1021/acsami.2c05918
ACS Appl. Mater. Interfaces 2022, 14, 35504−35512

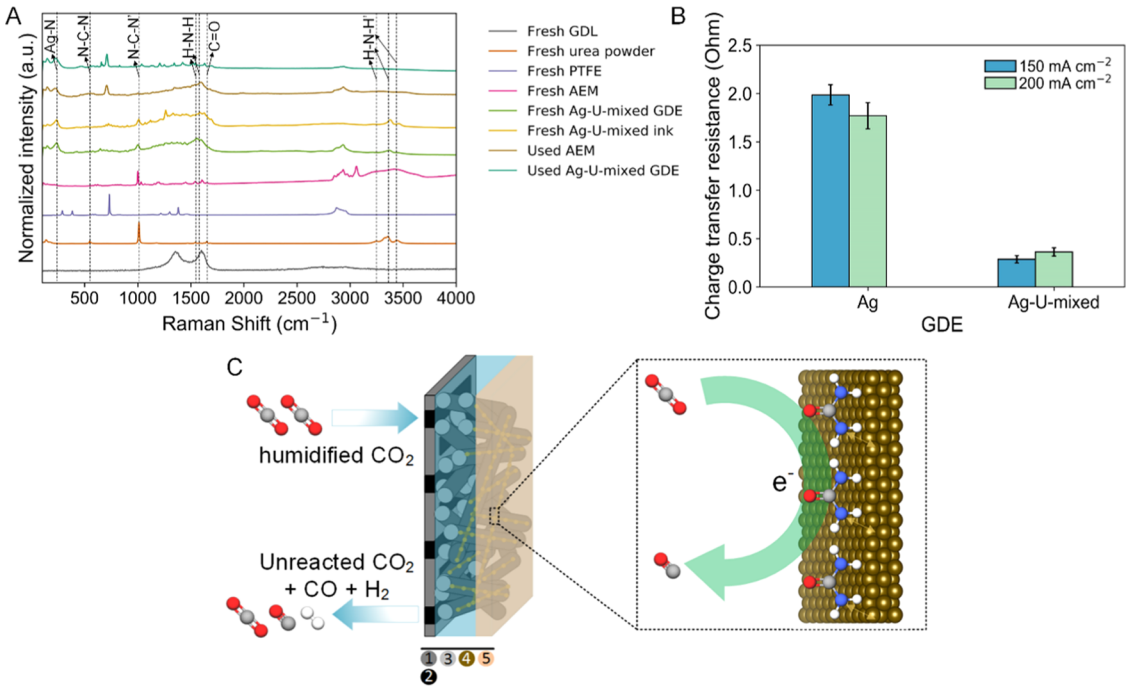


**Figure 3.** (A) Comparison of the Raman spectra of different species including fresh GDL, fresh urea powder, fresh PTFE, fresh AEM, fresh Ag-U-mixed, fresh Ag-U-mixed ink (dried in the air), used Ag-U-mixed AEM, and used Ag-U-mixed electrode. (B) Charge transfer resistances by modeling impedance experiments during $CO_2R$ in Ag and Ag-U-mixed electrodes. The charge transfer resistance shown may be attributed to both the cathode and the anode. (C) An illustration of the cathode part of the MEA in which the availability of urea could help stabilize the $CO_2R$ intermediates, where 1 is the endplate, 2 is the gas flow field, 3 is the gas diffusion layer (GDL), 4 is the catalyst layer, and 5 is the membrane. Atom colors in (C) are O in red, C in gray, N in blue, and H in white.

mixed GDE to the spectra of urea, PTFE, bare GDL 240, the Sustainion AEM, and preparation of the catalyst ink (Figure 3A). The fresh urea powder has several distinctive peaks at 548, 1011, 1541, 1581, and 1649 cm$^{-1}$, corresponding to the N−C−N bending mode,[40] N−C−N symmetric stretching mode,[40] −$NH_2$ bending mode,[40] H-bonded C═O stretching mode,[40] and H-free C═O stretching mode,[40] respectively. The fresh urea powder has three additional peaks at 3245, 3355, and 3437 cm$^{-1}$, which are relevant to the antisymmetric and symmetric −$NH_2$ stretching modes. These peak frequencies agree with the literature data.[40,41]

The urea-related peaks in the fresh Ag-U-mixed electrode are positioned at 548, 1001, 1558, 1592, 3216, 3366, and 3459 cm$^{-1}$. A slight shift of urea peaks in the fresh Ag-U-mixed GDE may be attributed to the interaction of urea with Ag.[42] Similarly, we observed the urea-related peaks in the dried Ag-U-mixed catalyst ink (fresh), the used Ag-U-mixed electrode, and the used AEM with the catalyst layer stuck on it after the $CO_2R$ (see Table S2 in the Supporting Information). However, we only observed very small −$NH_2$ anti/symmetric and symmetric stretching mode peaks over either the used Ag-U-mixed electrode or the used AEM. The low intensity of the −$NH_2$ stretching mode might be related to the low availability of urea left on the used Ag-U-mixed GDE after the $CO_2R$ test.

Interestingly, in all of the samples that contained urea and Ag, we observed a Raman peak at around 230 cm$^{-1}$ that was not observed in urea powders, GDL 240, PTFE, or AEM. This new peak is likely attributed to the Ag−urea vibrations, indicating chemisorption of urea on the Ag surface.[43] This analysis by Raman provides further evidence of strong interactions between urea and Ag through a Ag−amino group.

We used electrochemical impedance spectroscopy (EIS) to investigate the overall resistance and charge transfer resistances of Ag and Ag-U-mixed cells at different current densities. This EIS method follows similar approaches for MEA-based devices reported in the literature.[5,44] The high-frequency intercept of the EIS curves shown in Figure S11 (see experimental and fitted Nyquist plots) shows the overall cell resistance, while the semicircle represents the charge transfer resistance of both the cathodic and anodic half-cell reactions. Figure S11 shows slightly higher cell resistance in Ag GDE than that in the Ag-U-mixed GDE at 200 mA·cm$^{-2}$, meaning that the availability of urea at the cathode−membrane interface promotes ion transport across the AEM. In Figure 3B, the charge transfer resistance ($R_{CT}$) calculated from the EIS is significantly larger in Ag GDE than that in the Ag-U-mixed GDE. Although the $R_{CT}$ data shown in Figure 3B account for resistances at both the cathode and the anode, we used the same type of anode (fresh each time) in each experiment, so here, a decrease in $R_{CT}$ for the Ag-U-mixed electrode can only be due to the change in the cathode. The trends of $R_{CT}$ values in both Ag and Ag-U-mixed GDEs are consistent with the cell potential data shown in Figure 1C, meaning that a high $R_{CT}$ value increases the cell potential. The large $R_{CT}$ for untreated Ag GDE may result from the insufficient availability of $K^+$ ions at the cathode for efficient $CO_2R$, which is known to be an issue when using dilute anolytes. In contrast, we propose that the lower $R_{CT}$ for the Ag-U-mixed GDE observed with the same dilute anolyte may relate to urea enhancing $CO_2R$ on the Ag catalyst surface. (Figure 3C)

We tested this hypothesis on the role of urea in promoting $CO_2R$ using density functional theory (DFT) simulations. A detailed description of the DFT calculations is provided in the


https://doi.org/10.1021/acsami.2c05918
ACS Appl. Mater. Interfaces 2022, 14, 35504−35512

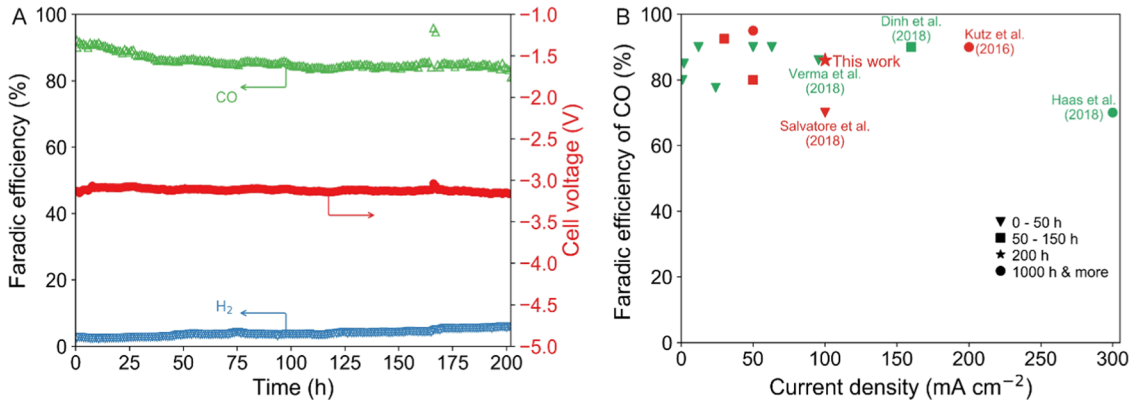


**Figure 4.** (A) Faradic efficiency of CO and $H_2$ and cell voltage as a function of time for the 200 h $CO_2R$ durability test at a constant current density of 100 mA·cm$^{-2}$ (cathode: Ag-U-mixed GDE; anode: $IrO_2$-based GDE; catholyte: humidified $CO_2$ at 60 sccm, anolyte: 10 mM $KHCO_3$ at 1 ml/min; and membrane: Sustainion AEM). (B) summary of the long-term electrode durability test showing the faradic efficiency of CO as a function of current density over various catalysts tested in liquid-fed flow cells (green color) and MEA cells (red color). The details of the literature work shown in (B) are provided in Table S3.

Supporting Information. Considering the Ag catalyst in our study is mainly dominated by the Ag(111) facets (see Figure S12), we used a periodic Ag(111) surface with seven layers and 112 Ag atoms (named $Ag_{112}$) as our DFT model. The modeling identified that the urea molecules could strongly interact with Ag(111) by sitting in a horizontal orientation on the Ag(111) surface with a urea−$Ag_{112}$ binding energy of −0.68 eV and a binding distance of 2.86 Å. (see Figure S13) This finding is consistent with our experimental observations from XPS and Raman spectroscopy.

$CO_2$ electrolysis to CO is reported to proceed via successive proton-coupled electron transfer (PCET) steps associated with the formation of *CO and *COOH intermediates.[45,46] We, therefore, calculated the binding energies, minimum binding distances, and Gibbs free energies of the key intermediates in $CO_2R$ and HER (including *H, *CO, and *COOH) over the optimized $Ag_{112}$ structure (see Figures S14 and S15) with and without urea adsorption. The DFT results summarized in Table S3 show that the urea-adsorbed Ag structure has a Gibbs binding energy 17% higher with *COOH and 15.3% higher with *CO compared with the bare Ag structure. A strengthened interaction with *COOH relative to that with *CO could contribute to the enhancement of $CO_2R$ to CO, as observed from the experiment (Figure 1). Our conclusion here that the amino group stabilizes the reaction intermediates is consistent with the literature.[10] Moreover, we found only a small difference in the Gibbs binding energies with *H for urea-adsorbed Ag (−1.47 eV) and bare Ag (−1.45 eV), meaning that urea shows a negligible thermodynamic effect in inhibiting HER. In this case, the experimentally observed HER suppression by urea may be due to other effects of urea on the local reaction environment at the cathode, such as influencing local pH.

The direct measurement of local pH in the MEA electrolyzer is not feasible, and the prediction of local pH by simulations is computationally intensive and uncertain. However, we can make relative inferences about local pH conditions for the untreated Ag GDE and the Ag-U-mixed GDE from the rate of carbonate formation from the reaction of acidic $CO_2$ with $OH^-$ during high current density $CO_2$ electrolysis. We estimated at 200 mA·cm$^{-2}$ current density that there was about 5% more $CO_2$ loss to carbonate with the Ag-U-mixed GDE than that with the untreated Ag GDE (see Table S4), which suggests that the local pH for the Ag-U-mixed GDE will be higher. The higher local pH limits proton availability and thus suppresses the HER. We caution that our $CO_2$ carbonation calculations using these experimental data can provide only a relative indication of local pH conditions. We also acknowledge that $CO_2$ loss via carbonation is a critical challenge for $CO_2$ electrolysis that needs to be addressed, for example, by introducing protons or optimizing the mass transport of water, ions, and gases.[11,47]

**3.3. Long-Term Electrolyzer Stability Test.** We tested the $CO_2R$ performance and stability of Ag-U-mixed MEA for 200 h at a constant current density of 100 mA·cm$^{-2}$ with no operational interruptions during the test. The cell was again supplied with a 10 mM $KHCO_3$ anolyte throughout the stability tests. In these tests, the initial $FE_{CO}$ of 91% dropped to about 85% in the first 25 h test, and then the selectivity remained stable at 85% for the remaining 175 h of the test (Figure 4A). $FE_{H_2}$ slowly increased with time but remained below 5% across the test. The CO selectivity loss in the first 25 h is likely due to the flooding of the catalyst from the loss of electrode wettability under applied potential.[48] The MEA cell maintained a relatively constant cell voltage of 3.116 ± 0.019 V over the durability test.

After 200 h operation, the selectivity of CO dropped from 85 to 74% in a sharp decline (Figure S16A) due to potassium bicarbonate ($KHCO_3$) precipitation in part of the gas flow field (see Figure S16B).[5] The salt precipitation is due to (i) $K^+$ diffusion through the AEM from the anolyte, (ii) limited water at the cathode, and (iii) the limited solubility of the carbonates.[6,29] We ruled out the potential contribution from the Ag deactivation because there is nearly no difference in the Ag 3d XPS spectra (see Figure S18) of the Ag-U-mixed electrodes before and after the stability test, which excludes the contribution from catalyst deactivation. Instead, we observed a rapid drop in the effluent flow rate from the cell after the 200 h test, where the degradation of $FE_{CO}$ follows a very similar trend. (Figure S17) The decreased flow rate reflects the blockage of $CO_2$ flow due to salt precipitation.

We also performed a long-term stability test with the untreated Ag GDE in our other work[49] (also shown in Figure S19) and found that the selectivity of CO was only around 62%, much less than what we observed with the Ag-U-mixed GDE (85%). In addition, the electrocatalytic performance


https://doi.org/10.1021/acsami.2c05918
ACS Appl. Mater. Interfaces 2022, 14, 35504−35512

cannot survive more than 100 h over Ag GDE, while the Ag-U-mixed GDE can run stably for almost double the time.

Although we had salt precipitation in the Ag-U-mixed GDE after the 200 h operation, the rate of salt precipitation and its impact on electrolyzer stability were much slower than those without urea. These results demonstrated that the urea-modified GDE could slow the salt precipitation process and enable highly selective and efficient $CO_2R$ when using a dilute anolyte because urea reduces the reliance of the electrolyzer on the transport of alkali cations to the cathode. Figure 4B compares our results with stability tests reported for $CO_2R$ to the CO electrolyzer including liquid-fed flow cells and vapor-fed MEA cells. The data are listed in Table S5 (where we also include additional examples from H-cell tests). The Ag-U-mixed cell outperforms most of the reported catalysts in terms of current density, energy efficiency, and $CO_2R$ test time while sustaining high $FE_{CO}$.

## 4. CONCLUSIONS

We demonstrated an alternative approach to improve both the efficiency and stability of $CO_2$ electrolysis based on MEA cells by enhancing $CO_2R$ and relieving the catalyst reliance on alkali cations. Our experiment and DFT calculations unveiled that the urea molecule can promote $CO_2R$ by stabilizing *COOH at the silver surface and optimizing the local reaction environment to minimize HER. As a result, the urea-modified GDE demonstrated a notable improvement in the $CO_2R$ performance of the MEA cells with 10 mM $KHCO_3$ as the anolyte, with a 1.3-fold enhancement of CO selectivity above 150 mA $cm^{-2}$ and a 2.8-fold improvement of energy efficiency at 200 mA $cm^{-2}$ compared to bare Ag GDE. The cell could also maintain a continuous stable operation at 100 mA $cm^{-2}$ for 200 h. Our work can be anticipated as a starting point to address the long-lasting issues faced by MEA-based technologies by modifying catalyst interfaces and the local reaction environment with molecular additives.

## ASSOCIATED CONTENT

### Supporting Information

The Supporting Information is available free of charge at https://pubs.acs.org/doi/10.1021/acsami.2c05918.

Description of density functional theory calculations including binding and Gibbs free energy calculations; schematic of how different Ag GDEs were examined in this work; schematic representation of the electrolyzer; formate detection using NMR; selectivity of $H_2$ while performing Ar electrolysis; energy efficiency plot; catalytic performance over different loadings of Ag-U-mixed GDEs; SEM data; high-resolution XPS data; photographs of the Ag-U-mixed GDE and the membrane before and after $CO_2R$; impedance data; XRD data; optimized structures (with top and side views) of urea@Ag112 and pristine Ag used in DFT calculations; photograph of salt precipitation in the cathode flow field; dependency of the outlet cathode flow rate on the selectivity of CO; long-term stability data using Ag GDE; and tables showing a summary of literature reports, Raman data, binding and Gibbs free energies data, $CO_2$ carbonation data, and summary of long-term stability tests in literature (PDF)

## AUTHOR INFORMATION


### Corresponding Authors

**Mengran Li** − *School of Chemical Engineering, the University of Queensland, 4072 Brisbane, Queensland, Australia; Department of Chemical Engineering, Faculty of Applied Sciences, Delft University of Technology, 2629 HZ Delft, The Netherlands;* orcid.org/0000-0001-7858-0533; Email: m.li6@uq.edu.au

**Thomas E. Rufford** − *School of Chemical Engineering, the University of Queensland, 4072 Brisbane, Queensland, Australia;* orcid.org/0000-0002-8865-7976; Email: t.rufford@uq.edu.au

### Authors

**Sahil Garg** − *School of Chemical Engineering, the University of Queensland, 4072 Brisbane, Queensland, Australia; Department of Physics, Technical University of Denmark, 2800 Kgs. Lyngby, Denmark*

**Tanveer Hussain** − *School of Chemical Engineering, the University of Queensland, 4072 Brisbane, Queensland, Australia; School of Science and Technology, University of New England, Armidale, New South Wales 2351, Australia*

**Mohamed Nazmi Idros** − *School of Chemical Engineering, the University of Queensland, 4072 Brisbane, Queensland, Australia*

**Yuming Wu** − *School of Chemical Engineering, the University of Queensland, 4072 Brisbane, Queensland, Australia*

**Xiu Song Zhao** − *School of Chemical Engineering, the University of Queensland, 4072 Brisbane, Queensland, Australia;* orcid.org/0000-0002-1276-5858

**Geoff G. X. Wang** − *School of Chemical Engineering, the University of Queensland, 4072 Brisbane, Queensland, Australia*

Complete contact information is available at: https://pubs.acs.org/10.1021/acsami.2c05918


### Notes

The authors declare no competing financial interest.

## ACKNOWLEDGMENTS

This research received funding from the HBIS Group, China, through the HBIS-UQ Innovation Centre for Sustainable Steel (ICSS) and Australian Research Council Linkage Project LP160101729 and Laureate Fellowship FL170100101. S.G., Y.W., and M.N.I. acknowledge scholarship support from the University of Queensland (UQ) Graduate School. The authors acknowledge the facilities and the scientific and technical assistance of the Australian Microscopy & Microanalysis Research Facility at the Centre for Microscopy and Microanalysis, UQ

## REFERENCES

(1) Spurgeon, J. M.; Kumar, B. A Comparative Technoeconomic Analysis of Pathways for Commercial Electrochemical $CO_2$ Reduction to Liquid Products. *Energy Environ. Sci.* **2018**, *11*, 1536−1551.

(2) Jouny, M.; Luc, W.; Jiao, F. General Techno-Economic Analysis of $CO_2$ Electrolysis Systems. *Ind. Eng. Chem. Res.* **2018**, *57*, 2165−2177.

(3) O'Brien, C. P.; Miao, R. K.; Liu, S.; Xu, Y.; Lee, G.; Robb, A.; Huang, J. E.; Xie, K.; Bertens, K.; Gabardo, C. M.; Edwards, J. P.; Dinh, C.-T.; Sargent, E. H.; Sinton, D. Single Pass $CO_2$ Conversion Exceeding 85% in the Electrosynthesis of Multicarbon Products via Local $CO_2$ Regeneration. *ACS Energy Lett.* **2021**, *6*, 2952−2959.

(4) Ozden, A.; Li, F.; García de Arquer, F. P.; Rosas-Hernández, A.; Thevenon, A.; Wang, Y.; Hung, S.-F.; Wang, X.; Chen, B.; Li, J.; Wicks, J.; Luo, M.; Wang, Z.; Agapie, T.; Peters, J. C.; Sargent, E. H.; Sinton, D. High-Rate and Efficient Ethylene Electrosynthesis Using a Catalyst/Promoter/Transport Layer. *ACS Energy Lett.* **2020**, *5*, 2811−2818.
(5) Endrődi, B.; Samu, A.; Kecsenovity, E.; Halmágyi, T.; Sebők, D.; Janáky, C. Operando Cathode Activation with Alkali Metal Cations for High Current Density Operation of Water-fed Zero-gap Carbon Dioxide Electrolysers. *Nat. Energy* **2021**, *6*, 439−448.
(6) Endrődi, B.; Kecsenovity, E.; Samu, A.; Darvas, F.; Jones, R. V.; Török, V.; Danyi, A.; Janáky, C. Multilayer Electrolyzer Stack Converts Carbon Dioxide to Gas Products at High Pressure with High Efficiency. *ACS Energy Lett.* **2019**, *4*, 1770−1777.
(7) Kutz, R. B.; Chen, Q.; Yang, H.; Sajjad, S. D.; Liu, Z.; Masel, I. R. Sustainion Imidazolium-Functionalized Polymers for Carbon Dioxide Electrolysis. *Energy Technol.* **2017**, *5*, 929−936.
(8) Ren, S.; Joulié, D.; Salvatore, D.; Torbensen, K.; Wang, M.; Robert, M.; Berlinguette, C. P. Molecular Electrocatalysts can Mediate Fast, Selective $CO_2$ Reduction in a Flow Cell. *Science* **2019**, *365*, 367−369.
(9) Weng, L.-C.; Bell, A. T.; Weber, A. Z. Towards Membrane-electrode Assembly Systems for $CO_2$ Reduction: A Modeling Study. *Energy Environ. Sci.* **2019**, *12*, 1950−1968.
(10) Monteiro, M. C. O.; Dattila, F.; Hagedoorn, B.; García-Muelas, R.; López, N.; Koper, M. T. M. Absence of $CO_2$ Electroreduction on Copper, Gold and Silver Electrodes Without Metal Cations in Solution. *Nat. Catal.* **2021**, *4*, 654−662.
(11) Huang, J. E.; Li, F.; Ozden, A.; Sedighian Rasouli, A.; García de Arquer, F. P.; Liu, S.; Zhang, S.; Luo, M.; Wang, X.; Lum, Y.; Xu, Y.; Bertens, K.; Miao, R. K.; Dinh, C.-T.; Sinton, D.; Sargent, E. H. $CO_2$ Electrolysis to Multicarbon Products in Strong Acid. *Science* **2021**, *372*, 1074−1078.
(12) Xu, Y.; Edwards, J. P.; Liu, S.; Miao, R. K.; Huang, J. E.; Gabardo, C. M.; O'Brien, C. P.; Li, J.; Sargent, E. H.; Sinton, D. Self-Cleaning $CO_2$ Reduction Systems: Unsteady Electrochemical Forcing Enables Stability. *ACS Energy Lett.* **2021**, *6*, 809−815.
(13) Tamura, J.; Ono, A.; Sugano, Y.; Huang, C.; Nishizawa, H.; Mikoshiba, S. Electrochemical Reduction of $CO_2$ to Ethylene Glycol on Imidazolium Ion-terminated Self-assembly Monolayer-modified Au Electrodes in an Aqueous Solution. *Phys. Chem. Chem. Phys.* **2015**, *17*, 26072−26078.
(14) Wang, W.; Ning, H.; Yang, Z.; Feng, Z.; Wang, J.; Wang, X.; Mao, Q.; Wu, W.; Zhao, Q.; Hu, H.; Song, Y.; Wu, M. Interface-induced Controllable Synthesis of $Cu_2O$ Nanocubes for Electro-reduction $CO_2$ to $C_2H_4$. *Electrochim. Acta* **2019**, *306*, 360−365.
(15) Zarandi, R. F.; Rezaei, B.; Ghaziaskar, H. S.; Ensafi, A. A. Electrochemical Reduction of $CO_2$ to Ethanol using Copper Nanofoam Electrode and 1-butyl-3-methyl-imidazolium Bromide as the Homogeneous Co-catalyst. *J. Environ. Chem. Eng.* **2019**, *7*, No. 103141.
(16) Khadhraoui, A.; Gotico, P.; Boitrel, B.; Leibl, W.; Halime, Z.; Aukauloo, A. Local Ionic Liquid Environment at a Modified Iron Porphyrin Catalyst Enhances the Electrocatalytic Performance of $CO_2$ to CO Reduction in Water. *Chem. Commun.* **2018**, *54*, 11630−11633.
(17) Ummireddi, A. K.; Sharma, S. K.; Pala, R. G. S. Inhibition of Hydrogen Evolution Without Debilitating Electrochemical $CO_2$ Reduction via the Local Suppression of Proton Concentration and Blocking of Step-edges by Pyridine Functionalization on Cu Electrocatalysts. *Catal. Sci. Technol.* **2021**, *11*, 4857−4865.
(18) Garg, S.; Li, M.; Rufford, T. E.; Ge, L.; Rudolph, V.; Knibbe, R.; Konarova, M.; Wang, G. G. X. Catalyst−Electrolyte Interactions in Aqueous Reline Solutions for Highly Selective Electrochemical $CO_2$ Reduction. *ChemSusChem* **2020**, *13*, 304−311.
(19) Kim, C.; Eom, T.; Jee, M. S.; Jung, H.; Kim, H.; Min, B. K.; Hwang, Y. J. Insight into Electrochemical $CO_2$ Reduction on Surface-Molecule-Mediated Ag Nanoparticles. *ACS Catal.* **2017**, *7*, 779−785.
(20) Kim, C.; Jeon, H. S.; Eom, T.; Jee, M. S.; Kim, H.; Friend, C. M.; Min, B. K.; Hwang, Y. J. Achieving Selective and Efficient Electrocatalytic Activity for $CO_2$ Reduction Using Immobilized Silver Nanoparticles. *J. Am. Chem. Soc.* **2015**, *137*, 13844−13850.
(21) Buckley, A. K.; Lee, M.; Cheng, T.; Kazantsev, R. V.; Larson, D. M.; Goddard, W. A., Iii; Toste, F. D.; Toma, F. M. Electrocatalysis at Organic−Metal Interfaces: Identification of Structure−Reactivity Relationships for $CO_2$ Reduction at Modified Cu Surfaces. *J. Am. Chem. Soc.* **2019**, *141*, 7355−7364.
(22) Barton Cole, E.; Lakkaraju, P. S.; Rampulla, D. M.; Morris, A. J.; Abelev, E.; Bocarsly, A. B. Using a One-Electron Shuttle for the Multielectron Reduction of $CO_2$ to Methanol: Kinetic, Mechanistic, and Structural Insights. *J. Am. Chem. Soc.* **2010**, *132*, 11539−11551.
(23) Banerjee, S.; Han, X.; Thoi, V. S. Modulating the Electrode−Electrolyte Interface with Cationic Surfactants in Carbon Dioxide Reduction. *ACS Catal.* **2019**, *9*, 5631−5637.
(24) Banerjee, S.; Zhang, Z.-Q.; Hall, A. S.; Thoi, V. S. Surfactant Perturbation of Cation Interactions at the Electrode−Electrolyte Interface in Carbon Dioxide Reduction. *ACS Catal.* **2020**, *10*, 9907−9914.
(25) Lim, H.-K.; Shin, H.; Goddard, W. A.; Hwang, Y. J.; Min, B. K.; Kim, H. Embedding Covalency into Metal Catalysts for Efficient Electrochemical Conversion of $CO_2$. *J. Am. Chem. Soc.* **2014**, *136*, 11355−11361.
(26) Fang, Y.; Cheng, X.; Flake, J. C.; Xu, Y. $CO_2$ Electrochemical Reduction at Thiolate-modified Bulk Au Electrodes. *Catal. Sci. Technol.* **2019**, *9*, 2689−2701.
(27) Ma, S.; Luo, R.; Gold, J. I.; Yu, A. Z.; Kim, B.; Kenis, P. J. A. Carbon Nanotube Containing Ag Catalyst Layers for Efficient and Selective Reduction of Carbon Dioxide. *J. Mater. Chem. A* **2016**, *4*, 8573−8578.
(28) Larrazábal, G. O.; Strøm-Hansen, P.; Heli, J. P.; Zeiter, K.; Therkildsen, K. T.; Chorkendorff, I.; Seger, B. Analysis of Mass Flows and Membrane Cross-over in $CO_2$ Reduction at High Current Densities in an MEA-Type Electrolyzer. *ACS Appl. Mater. Interfaces* **2019**, *11*, 41281−41288.
(29) Li, Y. C.; Yan, Z.; Hitt, J.; Wycisk, R.; Pintauro, P. N.; Mallouk, T. E. Bipolar Membranes Inhibit Product Crossover in $CO_2$ Electrolysis Cells. *Adv. Sustainable Syst.* **2018**, *2*, No. 1700187.
(30) Hsieh, Y.-C.; Betancourt, L. E.; Senanayake, S. D.; Hu, E.; Zhang, Y.; Xu, W.; Polyansky, D. E. Modification of $CO_2$ Reduction Activity of Nanostructured Silver Electrocatalysts by Surface Halide Anions. *ACS Appl. Energy Mater.* **2019**, *2*, 102−109.
(31) Xue, G.; Dai, Q.; Jiang, S. Chemical reactions of imidazole with metallic silver studied by the use of SERS and XPS techniques. *J. Am. Chem. Soc.* **1988**, *110*, 2393−2395.
(32) Ren, L.; Yang, F.; Wang, C.; Li, Y.; Liu, H.; Tu, Z.; Zhang, L.; Liu, Z.; Gao, J.; Xu, C. Plasma Synthesis of Oxidized Graphene Foam Supporting Pd Nanoparticles as a New Catalyst for One-pot Synthesis of Dibenzyls. *RSC Adv.* **2014**, *4*, 63048−63054.
(33) Akhter, S.; Zhou, X. L.; White, J. M. XPS Study of Polymer/organometallic Interaction: Trimethyl Aluminum on Polyvinyl Alcohol Polymer. *Appl. Surf. Sci.* **1989**, *37*, 201−216.
(34) Strohmeier, B. R. Evaluation Of Polymeric Standard Reference Materials For Monitoring The Performance Of X-Ray Photoelectron Spectrometers. *Appl. Surf. Sci.* **1991**, *47*, 225−234.
(35) Hantsche, H. High resolution XPS of organic polymers, the scienta ESCA300 database. By G. Beamson and D. Briggs, Wiley, Chichester 1992, 295 pp., hardcover, £ 65.00, ISBN 0-471-93592-1. *Adv, Mater.* **1992**, *5*, 778.
(36) Lee, T. H.; Rabalais, J. W. X-ray Photoelectron Spectra and Electronic Structure of Some Diamine Compounds. *J. Electron. Spectrosc. Relat. Phenom.* **1977**, *11*, 123−127.
(37) Thornburg, D. M.; Madix, R. J. Cleavage of NH Bonds by Active Oxygen on Ag(110): II. Selective Oxidation of Ethylamine to Acetonitrile. *Surf. Sci.* **1990**, *226*, 61−76.
(38) Ahn, S.; Klyukin, K.; Wakeham, R. J.; Rudd, J. A.; Lewis, A. R.; Alexander, S.; Carla, F.; Alexandrov, V.; Andreoli, E. Poly-Amide Modified Copper Foam Electrodes for Enhanced Electrochemical Reduction of Carbon Dioxide. *ACS Catal.* **2018**, *8*, 4132−4142.


https://doi.org/10.1021/acsami.2c05918
*ACS Appl. Mater. Interfaces* 2022, 14, 35504−35512

(39) Cao, Z.; Zacate, S. B.; Sun, X.; Liu, J.; Hale, E. M.; Carson, W. P.; Tyndall, S. B.; Xu, J.; Liu, X.; Liu, X.; Song, C.; Luo, J.-h.; Cheng, M.-J.; Wen, X.; Liu, W. Tuning Gold Nanoparticles with Chelating Ligands for Highly Efficient Electrocatalytic $CO_2$ Reduction. *Angew. Chem., Int. Ed.* **2018**, *57*, 12675−12679.
(40) Frost, R. L.; Kristof, J.; Rintoul, L.; Kloprogge, J. T. Raman Spectroscopy of Urea and Urea-intercalated Kaolinites at 77 K. *Spectrochim. Acta, Part A* **2000**, *56*, 1681−1691.
(41) Keuleers, R.; Desseyn, H. O.; Rousseau, B.; Van Alsenoy, C. Vibrational Analysis of Urea. *J. Phys. Chem. A* **1999**, *103*, 4621−4630.
(42) Ferraro, J. R.; Nakamoto, K.; Brown, C. W. Basic Theory. In *Introductory Raman Spectroscopy*, 2nd ed.; Ferraro, J. R.; Nakamoto, K.; Brown, C. W., Eds.; Academic Press, 2003; Chapter 1, pp 1−94.
(43) Suh, J. S.; Moskovits, M. Surface-enhanced Raman spectroscopy of Amino Acids and Nucleotide Bases Adsorbed on Silver. *J. Am. Chem. Soc.* **1986**, *108*, 4711−4718.
(44) Endrődi, B.; Kecsenovity, E.; Samu, A.; Halmágyi, T.; Rojas-Carbonell, S.; Wang, L.; Yan, Y.; Janáky, C. High Carbonate Ion Conductance of a Robust PiperION Membrane allows Industrial Current Density and Conversion in a Zero-gap Carbon Dioxide Electrolyzer Cell. *Energy Environ. Sci.* **2020**, *13*, 4098−4105.
(45) Yang, H.; Wu, Y.; Lin, Q.; Fan, L.; Chai, X.; Zhang, Q.; Liu, J.; He, C.; Lin, Z. Composition Tailoring via N and S Co-doping and Structure Tuning by Constructing Hierarchical Pores: Metal-Free Catalysts for High-Performance Electrochemical Reduction of $CO_2$. *Angew. Chem., Int. Ed.* **2018**, *57*, 15476−15480.
(46) Möller, T.; Ju, W.; Bagger, A.; Wang, X.; Luo, F.; Ngo Thanh, T.; Varela, A. S.; Rossmeisl, J.; Strasser, P. Efficient $CO_2$ to CO Electrolysis on Solid Ni−N−C Catalysts at Industrial Current Densities. *Energy Environ. Sci.* **2019**, *12*, 640−647.
(47) McCallum, C.; Gabardo, C. M.; O'Brien, C. P.; Edwards, J. P.; Wicks, J.; Xu, Y.; Sargent, E. H.; Sinton, D. Reducing the Crossover of Carbonate and Liquid Products During Carbon Dioxide Electroreduction. *Cell Rep. Phys. Sci.* **2021**, *2*, No. 100522.
(48) Li, M.; Idros, M. N.; Wu, Y.; Burdyny, T.; Garg, S.; Zhao, X. S.; Wang, G.; Rufford, T. E. The Role of Electrode Wettability in Electrochemical Reduction of Carbon Dioxide. *J. Mater. Chem. A* **2021**, *9*, 19369.
(49) Garg, S.; Li, M.; Idros, M. N.; Wu, Y.; Wang, G.; Rufford, T. E. Is Maximising Current Density Always the Optimum Strategy in Electrolyser Design for Electrochemical CO2 Conversion to Chemicals? 2021.




https://doi.org/10.1021/acsami.2c05918
*ACS Appl. Mater. Interfaces* 2022, 14, 35504−35512